Journal of Computational Electronics 2: 275–279, 2003
© 2003 Kluwer Academic Publishers. *Manufactured in The Netherlands.*

Microscopic Description of Nanostructures Grown on (N11) Surfaces

MICHAEL POVOLOTSKYI, JÉRÔME GLEIZE, ALDO DI CARLO* AND PAOLO LUGLI
Department of Electronic Engineering, University of Rome "Tor Vergata" Via del Politecnico 1, 00133 Rome, Italy
dicarlo@ing.uniroma2.it

STEFAN BIRNER AND PETER VOGL
Walter Schottky Institute and Physics Department, Technical University of Munich, Am Coulombwall 3, 85748 Garching, Germany

Abstract. We report on a theoretical study of GaAs/InGaAs based nanostructures grown along the [N11] direction. The elastic deformations of the structures were calculated by means of the continuum elasticity theory, taking into account commensurability constraints at the interfaces. The strained atomic positions were derived, as well as the strain induced piezoelectric polarizations and electric fields. These data were used as an input for the calculation of the fundamental electronic transitions of our systems within the empirical tight-binding approach. These results are compared with the envelope function methods. We applied our approach to a (211) oriented InAs quantum dot embedded in a GaAs matrix, and to a (311) oriented InGaAs quantum wire, embedded in AlGaAs barriers. In both cases, we obtained a non-symmetric elastic deformation due to the lower symmetry of (N11)-oriented structures. Moreover, the atomic displacements and the strain induced piezoelectric potential induce a separation of the hole and electron wave functions, which are shifted from the dot center.

Keywords: tight binding, high index surfaces, piezoelectric field, nanostructures, atomistic description

1. Introduction

Semiconductor low dimensional heterostructures are widely used nowadays in electronic and optoelectronic devices [1]. Optoelectronic devices based on quantum wires (QWRs) and quantum dots (QDs), such as lasers and optical modulators have already demonstrated outstanding characteristics comparatively to the "bulk" systems. In the future, QDs are supposed to be the main elements of the single-electron applications such as quantum computer systems. A lot of experimental studies were performed over InGaAs/GaAs QWRs [2] and QDs [3] grown on (N11) substrates. These structures are very attractive because of the significant piezoelectric field, which is induced in such oriented systems due to the non-zero shear strain.

Theoretical studies of (N11) QDs and QWRs were performed in the framework of the envelope function approximations [4], as well as in more refined approaches [5].

In this paper we focus on the influence of strain and piezo-electric fields on the electronic properties of (N11) oriented QWRs and QDs. The paper is organized as follows: in Section 2 we describe the physical model and methods of numerical calculations, which we apply in Section 3 to particular examples of a QWR and a QD; the last Section 4 summarizes our results.

2. Theory and Numerical Methods

The elastic deformation of the structure is calculated by means of a continuum mechanical model [6,7]. We minimize the elastic energy of the heterostructure, taking into account commensurability constraints for high Miller index crystal planes [8]. We assume that the nanostructure is grown on a thick unstrained substrate and we neglect the converse piezo-electric effect.

*To whom correspondence should be addressed.

The computational procedure consists of the following steps: we introduce a rectangular non-homogeneous simulation grid over the whole structure in such a way that material interfaces coincide with the grid lines; in doing so, we introduce a "lattice-matching" deformation that transforms an unstrained unit cell in the quantum region (QWR or QD) in order to make it equal to the unit cell of the substrate material. In the case of cubic materials, the corresponding strain tensor is expressed as $\tilde{\varepsilon}_{ij} = \delta_{ij}\Delta a/a$. Then, we consider the vector displacements **u** of each grid node as independent variables, so that the strain tensor can be expressed as a linear function of them (here we have to use a discretization scheme that does not employ the central differences). At the end, using Hooke's law and appropriate boundary conditions, we can reduce the mechanical equilibrium equations to a linear system involving a symmetric sparse matrix. The solution of this system gives us the **u**'s, and, hence, the symmetric strain tensor:

$$\varepsilon_{ij} = \frac{1}{2}\left(\frac{\partial u_i}{\partial x_j} + \frac{\partial u_j}{\partial x_i}\right) + \tilde{\varepsilon}_{ij}. \qquad (1)$$

The piezo-electric polarization **P** is determined as a linear function of the strain tensor: $P_i = e_{ijk}\varepsilon_{jk}$. We assume that the built-in electric field is created by the piezo-electric charges ρ only ($\rho = -\mathrm{div}\,\mathbf{P}$). The built-in potential is calculated from Poisson's equation, discretized on the simulation grid. All of the above mentioned calculations were performed using the next**nano**^{3} software [9].

The starting point for the atomistic description of the heterostructure is building a conventional unit cell for a zincblende structure with a Bravais vector parallel to the growth direction. In our case the conventional cell's edges are parallel to the $[N11]$, $[\bar{2}NN]$ and $[0\bar{1}1]$ crystallographic directions, respectively. This conventional cell is then repeated in space in order to built a simulation supercell containing about 10^5 atoms. In order to find the equilibrium atom positions in the strained supercell, we start from the unstrained lattice of the substrate, and we interpolate linearly the displacements **u**, given on the "macroscopic" simulation grid, over the unstrained supercell's lattice sites. We must note that this procedure does not include the internal strain that changes the anion-cation bond length. Our work must then be considered as a first step towards a full description of the system on an atomistic level. A refinement of our model is indeed possible, by drawing an analogy between a frozen optical phonon and the internal strain displacements [10]. Work on this topic is in progress and will be published elsewhere.

We calculated the fundamental electronic transition energies within the empirical tight-binding (ETB) approach [11], using the $sp^3s^*d^5$ ETB parameterization derived by Jancu *et al.*, for interactions between nearest neighbours in the supercell [12]. Following these authors, we include strain effects by scaling the ETB parameters with respect to the cation-anion bond length, according to Harrison's rule. A precise description of the electronic energies of our systems also requires a relative offset between the valence bands of all the quantum regions included in the supercell. We included this in our simulation by shifting the onsite ETB parameters according to theoretical values of these offsets for bulk materials [13,14]. We note here that these offsets are only an approximation, as they were calculated for strained layers grown on (001) GaAs. Finally, the dangling bonds on the supercell's surfaces are saturated, in order to avoid the appeareance of surface states inside the heterostructure's gap. Due to the large size of the system, the ETB Hamiltonian is stored using a sparse matrix. Its diagonalization is performed following a Lanczos iterative procedure.

In addition to the ETB calculations, we also applied the effective mass approximation (EMA) to calculate the electronic transitions energies of our model systems. We consider that both the band edge energy and the effective mass are strain dependent, according to the model of Bir and Pikus [15]. All EMA calculations were performed using the Nextnano^3 package.

3. Results

We first consider an $In_{0.2}Ga_{0.8}As$ QWR grown on a (311) oriented GaAs substrate. Similar QWRs were successfully grown and investigated experimentally [2,16]. Indeed, the growth of an $In_{0.2}Ga_{0.8}As$ quantum well, surrounded by $Al_{0.5}Ga_{0.5}As$ barriers, can be performed on a patterned GaAs substrate, allowing for the appearance of a QWR region near the step on the substrate, as shown on Fig. 1. In Fig. 2, we show three relevant components of the strain tensor. The ε_{xx} and ε_{yy} components account for the lattice mismatch between the wire and barrier materials and the substrate. Indeed, the QWR undergoes an in-plane compression, as well as a tensile strain along the growth direction, which is consistent with a pseudomorphic structure strained on the in-plane GaAs lattice. In addition, we observe a

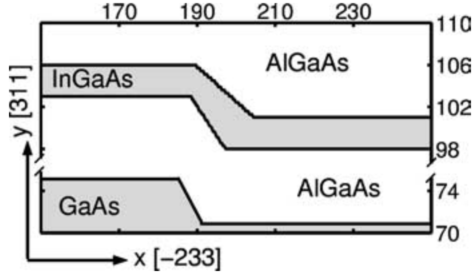

Figure 1. Schematic plot of the quantum wire cross-section by the $(01\bar{1})$ plane. Coordinates are given in nanometers.

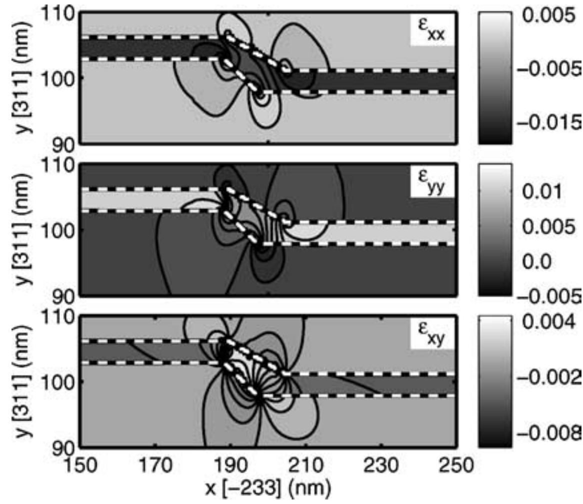

Figure 2. Contour plot of the strain tensor components ε_{xx},ε_{yy} and ε_{xy} in the cross-section of the QWR. The white dashed line shows the material interface between InGaAs and AlGaAs layers. The scale is different along x and y axes.

non-zero shear deformation ε_{xy}, which is a peculiarity of quantum wells grown on (N11) oriented substrates. We note that the strain is highly inhomogeneous at the step region, where the carriers tend to localize, and almost homegeneous far from it, as it is expected for the case of a quantum well [8]. Such strains induce piezo-electric charges at the step region and at the interfaces between the QWR and the barriers. The effect of the resulting piezo-electric field on the electron and hole states is illustrated in Fig. 3, where we plot the squared modulus of the EMA wave function of the ground state for two different cases: if the electric field is neglected and if it is included. We see that the piezo-electric field tends to separate the electrons and holes from each other.

We performed ETB calculations for this system, using a supercell containing 22,000 atoms, and included

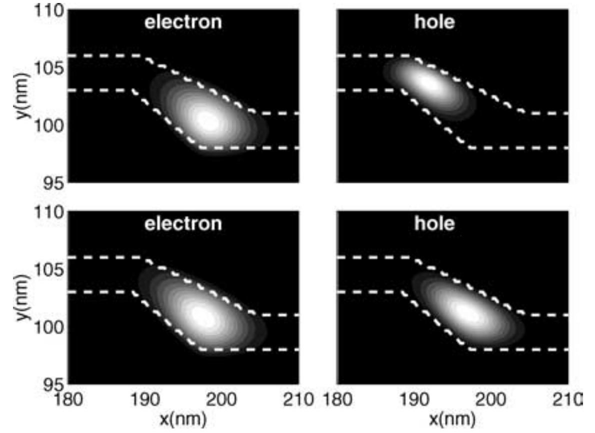

Figure 3. Modulus squared of the single-particle wave function for the ground state of electron and hole. The two lower figures correspond to the case if the piezo-electric field is neglected, the upper figures to the case if the field is taken into account. The axes are the same as in Fig. 2. Interfaces between wire and barrier are indicated by dashed lines.

spin orbit couplings. The alloy layers were treated in the virtual crystal approximation (VCA), by averaging all ETB parameters in the alloy regions according to Vegard's rule. A relevant bowing was added in the case of the $In_{0.2}Ga_{0.8}As$ region, ensuring that we obtain the same results as in Ref. [14] for the bulk. The supercell was isolated along the [311] and $[\bar{2}33]$ directions, and repeated periodically along the QWRs axis ($[0\bar{1}1]$ direction). Our results are summarized in Table 1, along with the EMA results. Both ETB and EMA results show the effect of the piezo-electric field, which is to reduce the fundamental electronic transition in the QWR by 4 to 8 meV. We note however a discrepancy between ETB and EMA results, the ETB energies being much larger than the EMA results. For comparison, ETB calculations were also performed for a supercell including only a quantum well-like region of the system, giving

Table 1. Empirical tight-binding and effective mass approximation calculations of the fundamental electronic transition energy in the quantum wire system described in Fig. 1. Calculations were performed including (unscreened) and without (screened) the piezo-electric potential.

	Screened potential		Unscreened potential	
	Tight binding	Effective mass	Tight binding	Effective mass
Energy (eV)	1.651	1.475	1.647	1.467

a transition energy of 1.950 eV. Both the QW-like and QWR transition energies are thus overestimated in our ETB simulation, which we attribute to our approximations in the atomistic descriptions, namely the purely external strains and an approximate band offset, which will be refined in further calculations.

Next, we consider an InAs truncated pyramid, on an InAs wetting layer, surrounded by a GaAs matrix, grown on a (211) oriented substrate. The geometry of the dot, described in Fig. 4, is that of a 2 nm high truncated pyramid, with square bases (10 nm wide at the bottom and 2 nm wide at the top of the dot). Due to the non-symmetric character of the growth axis, all components of the strain tensor are non-zero. In Fig. 5(a), we show a distribution of the strain tensor components ε_{xx} and ε_{yy} over the cross-section of the QD. It's noteworthy that strain distribution is not symmetric, despite the symmetric dot shape. This is again due to the high index of the QD growth direction. Fig. 5(b) shows the density of the piezo-electric charge calculated for the case if the GaAs substrate is terminated by a cation plane (A-type of the interface). In the opposite case (B-type of the interface), the charge density changes its sign. EMA fundamental transitions are given in Table 2, for screened and unscreened electric fields, and for both A-type and B-type interfaces. The effect of the piezoelectric field is clearly observed, as a red shift of 250 to 300 meV occurs if fields are included in the simulation. We also note that the type of interface plays a significant part, since an additional 60 meV red shift is obtained when the interface is changed from A-type to B-type.

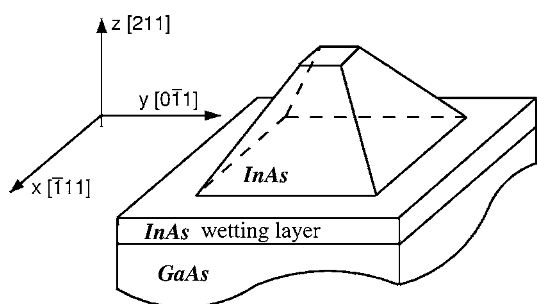

Figure 4. Schematic plot of the quantum dot.

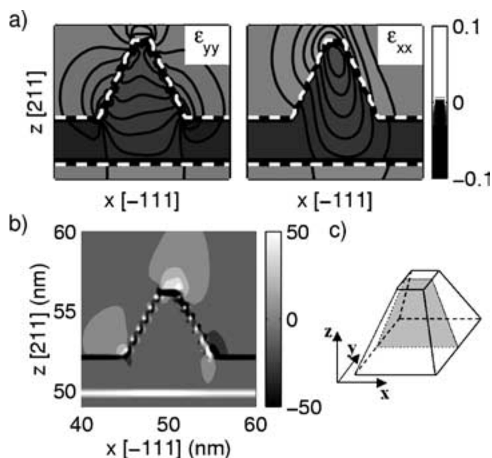

Figure 5. (a) Contour plot of the strain tensor components ε_{xx} and ε_{yy} in the cross-section of the QD. Interfaces between InAs and GaAs are indicated by white dashed lines. (b) Piezo-charge distribution in the cross section of the QD. The units are 10^{18} e/cm^3. (c) Schematic plot of the cross section plane refered to in (a) and (b).

Table 2. Effective mass approximation calculation of the fundamental electronic transition energy in the InAs quantum dot system described in Fig. 4. Calculations were performed including (unscreened) and without (screened) the piezoelectric potential. A-type and B-type interfaces were considered for the piezo electric potentials.

		Unscreened potential	
	Screened potential	A-type	B-type
Energy (eV)	1.019	0.756	0.695

4. Conclusions

In this paper we demonstrated an approach to the microscopic description of nanoscale devices, that takes into account strain, piezo-electric charge and atomic structure. This technique can be applied to any growth orientation, pure materials or alloys. An application to the particular case of (N11) oriented QWRs and a QDs was given, showing the influence of built-in piezoelectric fields on the electronic transition energies in such systems.

Future development of the method will include a microscopic calculation of the internal strain, in order to obtain a precise quantitative description of nanosystems on an atomistic scale, using empirical tight-binding techniques.

Acknowledgments

The work was financially supported by the fund PAIS "PIE" of INFM (Italy) and by the E.U. project "CLERMONT".

References

1. Z.I. Alferov, *Rev. Mod. Phys.*, **73**, 767 (2001).
2. R. Nötzel, M. Ramsteiner, Z. Niu, H.-P. Schönherr, L. Däweritz, and K.H. Ploog, *Appl. Phys. Lett*, **70**, 1578 (1997).
3. S. Sanguinetti, M. Gurioli, E. Grilli, M. Guzzi, and M. Henini, *Appl. Phys. Lett*, **77**, 2979 (2000).
4. O. Stier, M. Grundmann, and D. Bimberg, *Phys. Rev. B*, **59**, 5688 (1998).
5. A. Di Carlo, *Semicond. Sci. Technol.*, **18**, R1 (2003).
6. C. Pryor, M.-E. Pistol, and L. Samuelson, *Phys. Rev. B*, **56**, 10404 (1997).
7. B. Jogai, *J. Appl. Phys.*, **88**, 5050 (2000).
8. L. De Caro and L. Tapfer, *Phys. Rev. B*, **48**, 2298 (1993).
9. next**nano**^{3} device simulation package, see web site http://www.nextnano.de.
10. E. Anastassakis and M. Cardona, *Phys. Stat. Sol. (b)*, **104**, 589 (1981).
11. J.C. Slater and G.F. Koster, *Phys. Rev.*, **94**, 1498 (1954).
12. J.M. Jancu, R. Scholtz, F. Beltram, and F. Bassani, *Phys. Rev. B*, **57**, 6493 (1998).
13. I. Vurgaftman, J.R. Meyer, and L. R. Ram-Mohan, *J. Appl. Phys.*, **89**, 5815 (2001).
14. S.H. Wei and A. Zunger, *Appl. Phys. Lett.*, **72**, 2011 (2001).
15. C.Y.-P. Chao and S.L. Chuang, *Phys. Rev. B.*, **46**, 4110 (1992).
16. D. Alderighi, M. Zamfirescu, M. Gurioli, A. Vinattieri, M. Colocci, S. Sanguinetti, A. Di Carlo, M. Povolotskyi, and R. Nötzel, *Phys. Stat. Sol. (c)*, **0**, 1433 (2003).